

# New Polymer Syntheses Part 60: A Facile Synthetic Route to Polyamides Based on Thieno[2,3-*b*]thiophene and Their Corrosion Inhibition Behavior


Kamal I. Aly<sup>a</sup>, Amr H. Moustafa<sup>b\*</sup>, Essam K. Ahmed<sup>c</sup>, Hany M. Abd El-lateef<sup>d</sup>, Mohamed Gamal Mohamed<sup>a</sup>, and Sahar M. Mohamed<sup>c</sup>

<sup>a</sup> Polymer Research Lab, Chemistry Department, Faculty of Science, Assiut University, Assiut 71516, Egypt

<sup>b</sup> Chemistry Department, Faculty of Science, Sohag University, Sohag 82524, Egypt

<sup>c</sup> Chemistry Department, Faculty of Science, Minia University, El-Minia 61519, Egypt

<sup>d</sup> Chemistry Department, College of Science, King Faisal university, Al Hufuf, 31982 Al Hassa, Saudi Arabia

 Electronic Supplementary Information

**Abstract** Polyamides containing thieno[2,3-*b*]thiophene moiety were prepared *via* a simple polycondensation reaction of the diaminothieno[2,3-*b*]thiophene monomer **1a** with different kinds of diacid chlorides (including oxalyl, adipoyl, sebacoyl, isophthaloyl, terephthaloyl, 4,4'-azodibenzoyl, 3,3'-azodibenzoyl, *p*-phenylene diacryloyl) in the presence of LiCl and NMP as a solvent through low-temperature solution polycondensation. The chemical structures of model compound and synthesized polyamides were confirmed by FTIR, nuclear magnetic resonance spectroscopy (including <sup>1</sup>H-NMR and <sup>13</sup>C-NMR) and elemental analysis. In addition, the thermal stability, crystallinity structure and surface morphology of synthesized polyamides were characterized *via* thermogravimetric analysis (TGA), wide-angle X-ray diffraction analysis (WAXD) and scanning electron microscopy (SEM). Also, the corrosion inhibition behavior of selected examples of polyamides was investigated; the inhibitive effect of the investigated polymers for carbon steel in 1.0 mol·L<sup>-1</sup> HCl was studied using potentiodynamic polarization (PDP) and electrochemical impedance spectroscopy (EIS) methods. PDP results displayed that the polyamides containing thieno[2,3-*b*]thiophene moiety can be as mixed-type inhibitors. The inhibition efficiency (*P*, %) was found to be in the range from 67.13% to 96.01%. There is an increase in *P* by the synthesized polymers in comparison to the starting monomer. The adsorption of these polymers was found to obey Langmuir adsorption isotherm.

**Keywords** Thieno[2,3-*b*]thiophene; Polymer synthesis; Thermal properties; Industrial applications; Corrosion inhibition

**Citation:** Aly, K. I.; Moustafa, A. H.; Ahmed, E. K.; Abd El-lateef, H. M.; Mohamed, M. G.; Mohamed, S. M. New Polymer Syntheses Part 60: A Facile Synthetic Route to Polyamides Based on Thieno[2,3-*b*]thiophene and Their Corrosion Inhibition Behavior. Chinese J. Polym. Sci. 2018, 36(7), 835–847.

## INTRODUCTION

Polyamides are well known as high performance polymers due to their high thermal stability, high tensile strength, photo-curing ability, electronic conductivity, fluorescence, good chemical resistance, good mechanical properties, abrasion resistance, low friction coefficient and fire retarding property<sup>[1–6]</sup>. Most of them are widely used in different applications such as high strength, and high modulus fibers, high temperature coating and high efficiency semipermeable membrane<sup>[7]</sup>. However, they have some disadvantages such as high moisture absorption, poor low-temperature impact strength, poor dimensional stability and low heat distortion temperature<sup>[8, 9]</sup>. On the other hand, aromatic polyamides have been widely used in industry as a result of their high

thermal stability with a favorable balance of physical and chemical properties<sup>[10]</sup>, but most of them cannot be dissolved in organic solvents and do not melt. This makes them generally difficult or too expensive to process, thus restricting their applications<sup>[11]</sup>.

Recently, scientists have tried to improve the solubility and processibility of aromatic polyamides while maintaining their high thermal stability *via* introducing soft segments to the main chain of the polymers, breaking its symmetry and regularity, or introducing bulky groups to the side chain of the polymers<sup>[7, 11–24]</sup>.

The insertion of thienothiophene nucleus as a repeating unit into the polymer main chains will help them to gain new properties. One of the most important properties for polymers of thienothiophene is considered as conducting or semiconducting species that can be used in photovoltaic devices and applications due to the interesting electrochemical and optical properties<sup>[25, 26]</sup>. Furthermore, insertion of aliphatic chains, aromatic species, conjugated

\* Corresponding author: E-mail [amr\\_hassanegypt@ymail.com](mailto:amr_hassanegypt@ymail.com)  
[amr\\_hassanegypt@science.sohag.edu.eg](mailto:amr_hassanegypt@science.sohag.edu.eg)

Received September 17, 2017; Accepted December 9, 2017; Published online March 27, 2018

chains or aromatic azochromophores into the main chains of thienothiophene polymers will give them other properties such as their solubility, photochromic properties, photo sensitive liquid crystalline properties, in addition to their good thermal stability<sup>[22, 27–29]</sup>.

In this study, we synthesized and characterized novel eight polyamides **3a–3h** containing thienothiophene moiety *via* the reaction of 3,4-diaminothiopheno[2,3-*b*]thiophene-2,5-dicarbonitrile (**1a**) with different aliphatic, aromatic and azobenzene-diacid chlorides through low-temperature solution polycondensation technique<sup>[20, 30]</sup> (Scheme 1C). The major aim of this work is to investigate the effect of the inclusion of aliphatic chains, aromatic species and azo moieties on the thienothiophene polymers properties; also their thermal stability, solubility, viscometry, morphology and crystallinity were discussed. Finally, the corrosion inhibitive properties of selected polyamides were discussed *via* potentiodynamic polarization measurements (PDP).

## EXPERIMENTAL

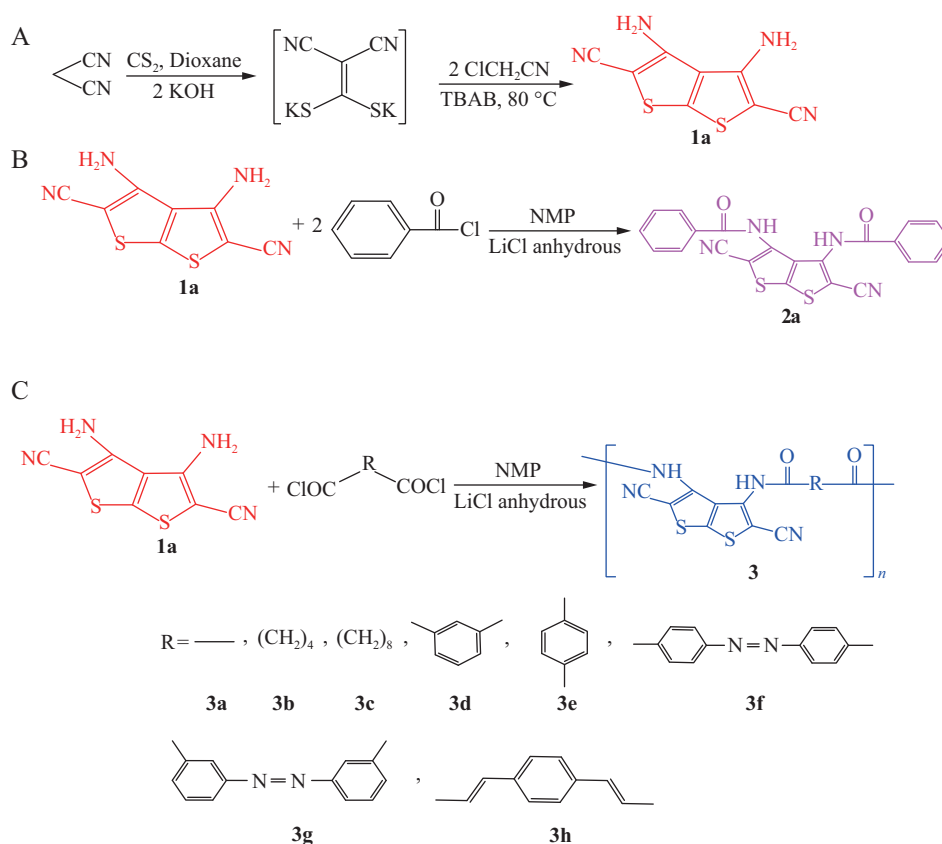
### Reagents and Materials

Commercially available malononitrile, carbon disulphide, chloroacetonitrile, *N*-methylpyrrolidone (NMP), ethanol (EtOH), chloroform (CHCl<sub>3</sub>), acetone, dimethylformamide (DMF) and anhydrous lithium chloride (LiCl) were purchased from Merck, Aldrich and Fluka and used without further purification. Dioxane from El-Nasr Chemical

Company (Egypt) was dried under sodium metal for 3 days then distilled (b.p. 101 °C). Benzoyl chloride from the same company was freshly distilled (b.p. 183–184 °C). Terephthaloyl chloride and isophthaloyl chloride (Aldrich) were freshly recrystallized from *n*-hexane (m.p. 83–84 °C and 40 °C, respectively). Adipoyl and sebacoyl dichlorides were freshly distilled at 125 °C/1.466 kPa, and at 182 °C/2.133 kPa, respectively<sup>[31]</sup>. Diacid chlorides were prepared according to the reported literature method<sup>[29, 32, 33]</sup>.

### Measurements

<sup>1</sup>H and <sup>13</sup>C nuclear magnetic resonance (NMR) spectra were recorded in DMSO-*d*<sub>6</sub> on a Bruker Bio Spin AG spectrometer at 400 and 100 MHz, respectively. For <sup>1</sup>H-NMR, chemical shifts ( $\delta$ ) were given in parts per million (ppm) with reference to tetramethylsilane (TMS) as an internal standard ( $\delta = 0$ ). For <sup>13</sup>C-NMR, TMS ( $\delta = 0$ ) or DMSO ( $\delta = 39.51$ ) was used as internal standard and spectra were obtained with complete proton decoupling. FTIR spectra of the monomers and polyamides films were recorded using a Bruker Tensor 27 FTIR spectrophotometer and the conventional KBr disk method; 32 scans were collected at a spectral resolution of 4 cm<sup>-1</sup>; the prepared films were sufficiently thin to obey the Beer-Lambert law. The molecular weights and polydispersity index of the synthesized polyamides were determined using a Waters 510 gel permeation chromatography (GPC) system equipped with a refractive index detector and three Ultrastaygel columns (100, 500, and 1000 Å) connected in series. DMF was the



**Scheme 1** Synthetic route to the target monomer **1a** (A), model compound **2a** (B) and polyamides **3a–3h** (C) containing thieno[2,3-*b*]thiophene

eluent, at a flow rate of 1 mL·min<sup>-1</sup>, at 40 °C. The solubility of polymers was examined using 0.02 g of polymer in 3–5 mL of solvent at room temperature. The inherent viscosity was determined with an Ubbelohde viscometer at 25 °C. WAXD profiles of the polymers were obtained at room temperature, with a Philips X-ray pw 1710 diffractometer and Ni-filtered Cu K $\alpha$  radiations. A triangular bent Si (111) single crystal was used to obtain a monochromated beam having a wavelength ( $\lambda$ ) of 1.32 Å. The morphologies of polymers were examined by scanning electron microscopy (SEM) using a Jeol JSM-5400 LV instrument. The thermal stabilities of the polyamides containing thieno[2,3-*b*]thiophene were measured using a TA Q-50 thermogravimetric analyzer operated under a N<sub>2</sub> atmosphere; a cured sample (*ca.* 5 mg) was placed in a Pt cell and heated at a rate of 10 °C·min<sup>-1</sup> from 30 °C to 600 °C under a N<sub>2</sub> flow of 60 mL·min<sup>-1</sup>. Carbon steel electrode with composition (wt%) C 0.17%, Si 0.19%, Ni 0.02%, Mn 0.70%, S 0.05%, Cr 0.02% and remainder Fe was used for the corrosion inhibition studies. The acid solution (1 mol·L<sup>-1</sup> HCl) was used as aggressive medium and prepared by dilution of AR grade HCl with double distilled water. The concentration range of polymers employed as corrosion inhibitors was 5 ppm to 50 ppm by weight. The electrochemical measurements were completed in a 1000 mL round-bottom cell fitted with a saturated calomel electrode as the reference electrode (SCE), a carbon steel working electrode, and a counter electrode of platinum sheet. After connecting all three electrode cells to the potentiostat, the potentiodynamic polarization curves were scanned from  $\pm 250$  mV with respect to the open circuit potential.  $E_{\text{corr}}$  was measured at a rate of 1.0 mV·s<sup>-1</sup>. The impedance measurements were performed at the open circuit potential with a frequency scan ranging from 100 kHz to 0.5 Hz and amplitude value of 10 mV. The impedance curves were fitted and the electrochemical equivalent circuit was obtained by Z-View software. All of measurements were conducted with VersaSTAT4 potentiostat/Galvanostat connected to laptop and accomplished at 50 °C.

#### Synthesis of 3,4-Diaminothieno[2,3-*b*]thiophene-2,5-dicarbonitrile (**1a**) (One Pot Multicomponent Synthesis)

To a mixture of malononitrile (6.60 g, 100 mmol) and carbon disulphide (9.0 mL, 150 mmol) in 80 mL of dry dioxane, powdered potassium hydroxide (11.20 g, 200 mmol) was added. The reaction mixture was stirred at room temperature for 1 h. Then, chloroacetonitrile (12.70 mL, 201 mmol) and tetrabutylammonium bromide (20 mmol) were added and the reaction mixture was further stirred at 80 °C for 4 h. After completion of the reaction, the mixture was poured into ice cold water and the formed precipitate was filtered, dried, and washed with hot ethanol to give a brown solid; yield: 92%, m.p. > 300 °C<sup>[34, 35]</sup>. R<sub>f</sub> value 0.40 (CHCl<sub>3</sub>:MeOH; 20:1). FTIR (KBr, cm<sup>-1</sup>): 3302 and 3204 (NH stretch), 2195 (C $\equiv$ N stretch) (See Fig. S1, in the electronic supplementary information, ESI). <sup>1</sup>H-NMR (400 MHz, DMSO-d<sub>6</sub>,  $\delta$ , ppm): 6.82 (s, 4H, 2NH<sub>2</sub>) (Fig. S2, in ESI). <sup>13</sup>C-NMR (100 MHz, DMSO-d<sub>6</sub>,  $\delta$ , ppm): 150.5, 146.9, 126.1, 115.9, 78.7 (Fig. S3, in ESI). Anal. Calcd. for C<sub>8</sub>H<sub>4</sub>N<sub>4</sub>S<sub>2</sub> (220): C 43.62; H 1.83;

N 25.44. Found: C 43.83; H 1.80; N 25.30.

#### Synthesis of *N,N'*-(2,5-dicyanothieno[2,3-*b*]thiophene-3,4-diyl) dibenzamide (**2a**) as Model Compound

Compound **1a** (1.98 g, 9 mmol) in LiCl/NMP (0.60 g in 40 mL) was stirred under nitrogen in an ice bath for 30 min, then benzoyl chloride (2.09 mL, 18 mmol) was slowly added and the reaction mixture was continued stirred at 0 °C for 8 h. The temperature of the reaction was then raised into room temperature with stirring for 6 h. After completion of the reaction (monitored with), the mixture solution was poured into ice cold water and the formed precipitate was collected by filtration, washed with aqueous NaHCO<sub>3</sub> then distilled water and recrystallized from ethanol to afford white solid; yield: 80%, m.p. > 300 °C. FTIR (KBr, cm<sup>-1</sup>): 3239 (N–H stretch), 3058, 3032 (C–H aromatic), 2220 (C $\equiv$ N stretch), 1656 (C=O stretch), (See Fig. S5 in ESI). <sup>1</sup>H-NMR (400 MHz, DMSO-d<sub>6</sub>,  $\delta$ , ppm): 10.60 (s, 2H, 2NH), 7.78 (d,  $J$  = 7.4 Hz, 4H, CH<sub>arom.</sub>), 7.51 (t,  $J$  = 7.4 Hz, 2H, CH<sub>arom.</sub>), 7.32 (t,  $J$  = 7.76 Hz, 4H, CH<sub>arom.</sub>) (Fig. S6, in ESI). <sup>13</sup>C-NMR (100 MHz, DMSO-d<sub>6</sub>,  $\delta$ , ppm): 165.9, 145.1, 138.5, 134.9, 132.9, 132.6, 128.7, 128.2, 113.3, 107.4 (Fig. S7, in ESI). Anal. Calcd. for C<sub>22</sub>H<sub>12</sub>N<sub>4</sub>O<sub>2</sub>S<sub>2</sub> (428.48): C 61.67; H 2.82; N 13.08; Found: C 61.77; H 2.72; N 13.20.

#### General Procedure for Synthesis of Polyamides Containing Thieno[2,3-*b*]thiophene **3a–3h**

In a 250 mL three-necked round-bottomed flask equipped with a magnetic stirrer, dry nitrogen inlet and outlet and a dropper, 3,4-diaminothieno[2,3-*b*]thiophene-2,5-dicarbonitrile (**1a**) (1.98 g, 9 mmol) in LiCl/NMP (0.60 g in 40 mL) was stirred for 30 min in an ice bath and a solution of the appropriate diacid chlorides (9 mmol) in NMP (5 mL) was added dropwise while maintaining stirred reaction mixture at 0 °C. After completion addition, the mixture was continuously stirred under nitrogen at 0 °C for 8 h and at room temperature for 6 h. The reaction mixture was poured into methanol (60 mL) and the formed fibrous precipitate was filtered off, washed with diluted HCl solution to remove entrapped NMP solvent, dried, washed with a solution of NaHCO<sub>3</sub> and finally with hot ethanol.

##### Polyamide **3a**

It was obtained *via* the polymerization of monomer **1a** (1.98 g, 9 mmol) with oxalyl chloride (0.78 mL, 9 mmol) as white powder; yield 45%. FTIR (KBr, cm<sup>-1</sup>): 3206 (N–H stretch), 2215 (C $\equiv$ N stretch), 1674 (C=O). Anal. Calcd. for (C<sub>10</sub>H<sub>2</sub>N<sub>4</sub>O<sub>2</sub>S<sub>2</sub>)<sub>n</sub> (%): C 43.79; H 0.73; N 20.43; S 23.38. Found: C 43.67; H 0.80 ; N 20.55; S 23.29.

##### Polyamide **3b**

It was obtained *via* the polycondensation of monomer **1a** (1.98 g, 9 mmol) with adipoyl chloride (1.31 mL, 9 mmol) as white powder; yield 85%. FTIR (KBr, cm<sup>-1</sup>): 3210 (N–H stretch), 2941 and 2869 (C–H aliphatic), 2215 (C $\equiv$ N stretch), 1666 (C=O). Anal. Calcd. for (C<sub>14</sub>H<sub>10</sub>N<sub>4</sub>O<sub>2</sub>S<sub>2</sub>)<sub>n</sub> (%): C 50.90; H 3.05; N 16.96; S 19.41. Found: C 50.75; H 3.00; N 17.15; S 19.35.

##### Polyamide **3c**

It was obtained *via* the polymerization of monomer **1a** (1.98 g, 9 mmol) with sebacoyl chloride (1.92 mL, 9 mmol)

as white powder; yield 85%. FTIR (KBr,  $\text{cm}^{-1}$ ): 3213 (N–H stretch), 2925 and 2848 (C–H aliphatic), 2216 (C $\equiv$ N stretch), 1666 (C=O). Anal. Calcd. for  $(\text{C}_{18}\text{H}_{18}\text{N}_4\text{O}_2\text{S}_2)_n$  (%): C 55.94; H 4.69; N 14.50; S 16.59. Found: C 56.2; H 4.78; N 14.44; S 16.40.

#### Polyamide 3d

It was obtained *via* the polymerization of monomer **1a** (1.98 g, 9 mmol) with isophthaloyl chloride (1.83 g, 9 mmol) as white powder; yield 80%. FTIR (KBr,  $\text{cm}^{-1}$ ): 3210 (N–H stretch), 3055 (C–H aromatic), 2215 (C $\equiv$ N stretch), 1664 (C=O stretch).  $^1\text{H-NMR}$  (400 MHz,  $\text{DMSO-d}_6$ ,  $\delta$ , ppm): 10.81 (s, 2H, 2NH), 8.49 (s, 1H,  $\text{CH}_{\text{arom}}$ ), 7.94 (d,  $J = 7.6$  Hz, 2H,  $\text{CH}_{\text{arom}}$ ), 7.39 (t,  $J = 7.7$  Hz, 1H,  $\text{CH}_{\text{arom}}$ ).  $^{13}\text{C-NMR}$  (100 MHz,  $\text{DMSO-d}_6$ ,  $\delta$ , ppm): 165.5, 145.2, 139.0, 135.2, 132.8, 131.7, 128.8, 128.4, 113.2, 107.6. Anal. Calcd. for  $(\text{C}_{16}\text{H}_6\text{N}_4\text{O}_2\text{S}_2)_n$  (%): C 54.85; H 1.73; N 15.99; S 18.30. Found: C 54.98; H 1.90; N 15.73; S 18.19.

#### Polyamide 3e

It was obtained *via* the polymerization of monomer **1a** (1.98 g, 9 mmol) with terephthaloyl chloride (1.83 g, 9 mmol) as white powder; yield 80%. FTIR (KBr,  $\text{cm}^{-1}$ ): 3223 (N–H stretch), 3089 (C–H aromatic), 2215 (C $\equiv$ N stretch), 1657 (C=O stretch).  $^1\text{H-NMR}$  (400 MHz,  $\text{DMSO-d}_6$ ,  $\delta$ , ppm): 10.65 (s, 2H, 2NH), 7.76 (s, 4H,  $\text{CH}_{\text{arom}}$ ) (See Fig. S8, in ESI).  $^{13}\text{C-NMR}$  (100 MHz,  $\text{DMSO-d}_6$ ,  $\delta$ , ppm): 164.9, 145.1, 138.5, 135.6, 134.6, 128.2, 113.3, 107.9 (Fig. S9, in ESI). Anal. Calcd. for  $(\text{C}_{16}\text{H}_6\text{N}_4\text{O}_2\text{S}_2)_n$  (%): C 54.85; H 1.73; N 15.99; S 18.30. Found: C 54.92; H 1.65; N 15.60; S 18.41.

#### Polyamide 3f

It was obtained *via* the polymerization of monomer **1a** (1.98 g, 9 mmol) with 4,4'-diazene-1,2-diyl dibenzoyl chloride (2.76 g, 9 mmol) as red powder; yield 80%. FTIR (KBr,  $\text{cm}^{-1}$ ): 3190 (N–H stretch), 3050 (C–H aromatic), 2217 (C $\equiv$ N stretch), 1684 (C=O stretch), 1629 (N=N).  $^1\text{H-NMR}$  (400 MHz,  $\text{DMSO-d}_6$ ,  $\delta$ , ppm): 10.84 (br. s, 2H, 2NH), 7.96–7.88 (m, 4H,  $\text{CH}_{\text{arom}}$ ), 7.75–7.62 (m, 4H,  $\text{CH}_{\text{arom}}$ ) (See Fig. S10, in ESI).  $^{13}\text{C-NMR}$  (100 MHz,  $\text{DMSO-d}_6$ ,  $\delta$ , ppm): 166.8, 165.2, 154.4, 154.0, 145.2, 138.8, 135.2, 134.9, 133.7, 130.8, 129.6, 122.9, 122.7, 113.2, 109.9. Anal. Calcd. for  $(\text{C}_{22}\text{H}_{10}\text{N}_6\text{O}_2\text{S}_2)_n$  (%): C 58.14; H 2.22; N 18.49; S 14.11. Found: C 57.85; H 2.14; N 18.54; S 14.08.

#### Polyamide 3g

It was obtained *via* the polymerization of monomer **1a** (1.98 g, 9 mmol) with 3,3'-diazene-1,2-diyl dibenzoyl chloride (2.76 g, 9 mmol) as orange powder; yield 75%. FTIR (KBr,  $\text{cm}^{-1}$ ): 3313 (N–H stretch), 3030 (C–H aromatic), 2204 (C $\equiv$ N stretch), 1688 (C=O stretch), 1629 (N=N). Anal. Calcd. for  $(\text{C}_{22}\text{H}_{10}\text{N}_6\text{O}_2\text{S}_2)_n$  (%): C 58.14; H 2.22; N 18.49; S 14.11. Found: C 58.25; H 2.15; N 18.43; S 14.03.

#### Polyamide 3h

It was obtained *via* the polymerization of monomer **1a** (1.98 g, 9 mmol) with *p*-phenylene diacryloyl chloride (2.29 g, 9 mmol) as yellow powder; yield 80%. FTIR (KBr,  $\text{cm}^{-1}$ ): 3205 (N–H stretch), 3061 (C–H aromatic), 2217 (C $\equiv$ N stretch), 1659 (C=O stretch) (See Fig. S11, in ESI). Anal. Calcd. for  $(\text{C}_{22}\text{H}_{10}\text{N}_6\text{O}_2\text{S}_2)_n$  (%): C 59.69; H

2.50; N 13.92; S 15.93. Found: C 59.52; H 2.71; N 13.64; S 15.90.

## RESULTS AND DISCUSSION

### Synthesis of 3,4-Diaminothiopheno[2,3-*b*]thiophene-2,5-dicarbonitrile (Monomer, **1a**) and *N,N'*-(2,5-dicyanothiopheno[2,3-*b*]thiophene-3,4-diyl) dibenzamide (Model Compound, **2a**)

In this work, we synthesized a new class of polyamides based on thieno[2,3-*b*]thiophene unit and studied their physical properties and corrosion inhibition behavior. First, we prepared 3,4-diaminothiopheno[2,3-*b*]thiophene-2,5-dicarbonitrile (**1a**) according to the published procedure described earlier<sup>[34, 35]</sup> *via* one pot multicomponent reaction of malononitrile, carbon disulphide, potassium hydroxide, chloroacetonitrile and tetrabutylammonium bromide in 1,4-dioxane (Scheme 1A). The chemical structure of monomer **1a** was confirmed by FTIR,  $^1\text{H}$ -,  $^{13}\text{C}$ -NMR and elemental analysis. The FTIR spectrum of monomer **1a** (Fig. S1, in ESI) displays the characteristic peaks at 3302 and 3204  $\text{cm}^{-1}$  for  $\text{NH}_2$  group and 2195  $\text{cm}^{-1}$  for C $\equiv$ N stretching. The  $^1\text{H-NMR}$  spectrum of monomer **1a** (Fig. S2, in ESI) features signal at  $\delta = 6.82$  ppm representing the amino group ( $\text{NH}_2$ ) and the characteristic signal protons for  $\text{NH}_2$  disappeared in deuteration  $\text{D}_2\text{O}$  (as shown in Fig. S4, in ESI). Fig. S3 presents the  $^{13}\text{C-NMR}$  spectrum of monomer **1a** in  $\text{DMSO-d}_6$ ; the five signals of the aromatic and cyano groups appeared at  $\delta = 150.5, 146.9, 126.1, 115.9, 78.7$  ppm. Second, the model compound **2a** was synthesized by the reaction of monomer **1a** with benzoyl chloride (1:2 ratio), using anhydrous lithium chloride (LiCl) in NMP at room temperature (Scheme 1B). Also, we did FTIR,  $^1\text{H}$ -,  $^{13}\text{C}$ -NMR spectroscopy and elemental analyses to confirm its chemical structure. Fig. S5 (in ESI) displays FTIR spectrum of **2a** which showed disappearance of the characteristic absorption bands for amino group, while exhibited new characteristic absorption bands at 3239  $\text{cm}^{-1}$  (for NH, amide), 3058, 3032  $\text{cm}^{-1}$  (for C–H aromatic), and 1656  $\text{cm}^{-1}$  (for C=O, amide). Also, another characteristic absorption band assigned to C $\equiv$ N group appeared at 2220  $\text{cm}^{-1}$ . Its  $^1\text{H-NMR}$  spectrum in  $\text{DMSO-d}_6$  (Fig. S6, in ESI) showed singlet signal at  $\delta = 10.60$  ppm due to two NH groups and the signals of the aromatic protons appeared at  $\delta = 7.32, 7.51$  and 7.78 ppm. Its  $^{13}\text{C-NMR}$  spectrum is shown in Fig. S7 (in ESI). The characteristic carbon signals centered at  $\delta = 107.4, 113.3, 128.2, 128.7, 132.6, 132.9, 134.9, 138.5, 145.1$  ppm which are assigned to cyano group and aromatic carbons and at  $\delta = 165.9$  ppm representing carbonyl group. All this information from the FTIR,  $^1\text{H}$ - and  $^{13}\text{C}$ -NMR profiles is consistent with the successful synthesis of the monomer **1a** and model compound **2a**.

### Synthesis of Polyamides Containing Thieno[2,3-*b*]thiophene (**3a–3h**)

Generally, polyamides are synthesized by the polycondensation reaction of diamines with dicarboxylic acid or their corresponding diacid dichlorides *via* the direct phosphorylation polycondensation<sup>[36]</sup> or the low temperature

solution polycondensation in polar solvents such as DMAC, DMF or NMP<sup>[37]</sup>. As reported, the presence of LiCl-NMP solution is powerful enough to keep the growing polymer chain in solution as its molecular weight builds up<sup>[22]</sup>. After optimization of the reaction condition, a series of new polyamides (**3a–3h**) based on thieno[2,3-*b*]thiophene were obtained *via* low temperature solution polycondensation technique, by reaction of 3,4-diaminothieno[2,3-*b*]thiophene-2,5-dicarbonitrile (**1a**) with different kinds of aliphatic, aromatic and azobenzene-diacid chlorides namely: oxalyl, adipoyl, sebacoyl, isophthaloyl, terephthaloyl, 4,4'-diazene-1,2-diyl dibenzoyl, 3,3'-diazene-1,2-diyl dibenzoyl, and *p*-phenylene diacryloyl chlorides in the presence of NMP as a solvent and LiCl (Scheme 1C). During the polymerization reaction, the liberated HCl gas was absorbed by NMP which acted as good acid acceptor.

The molecular structures of the obtained polyamides **3a–3h** were confirmed by spectroscopic methods including FTIR, <sup>1</sup>H-NMR and <sup>13</sup>C-NMR spectroscopy. Fig. 1 presents FTIR spectra of polyamides **3a–3g**. As shown in Fig. 1, all synthesized polyamides showed the presence of new absorption bands corresponding to N–H stretching and CO<sub>amide</sub> groups at 3190–3223 and 1657–1688 cm<sup>-1</sup>, respectively. In addition, there is a band at 2204–2217 cm<sup>-1</sup> for C≡N groups. Polyamides **3b** and **3c** exhibited characteristic absorption bands at 2848–2941 cm<sup>-1</sup> for C–H<sub>aliph.</sub>. In addition, an azo group band (N=N) was seen for polyamides **3f** and **3g**.

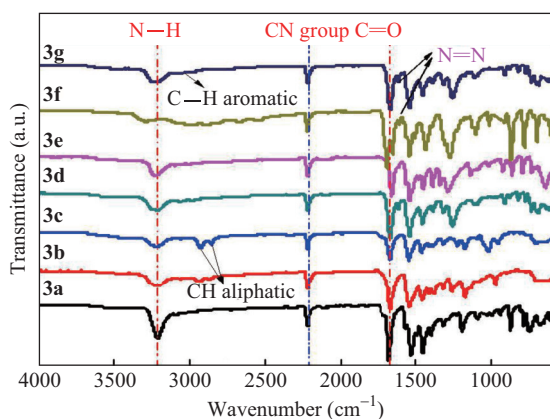


Fig. 1 FTIR spectra of polyamides **3a–3g**, recorded at room temperature

The <sup>1</sup>H-NMR and <sup>13</sup>C-NMR spectra for polyamide **3d** in DMSO-*d*<sub>6</sub> are presented in Figs. 2 and 3, respectively. <sup>1</sup>H-NMR spectrum of polymer **3d** showed the presence of singlet signal at  $\delta = 10.81$  ppm due to proton of NH group, which disappeared in deuteration D<sub>2</sub>O. In addition, the presence of singlet signal at  $\delta = 8.49$  ppm, doublet and triplet signals at  $\delta = 7.94$  and 7.39 ppm represented aromatic protons, respectively. The <sup>13</sup>C-NMR spectrum of **3d** (Fig. 3) showed nine signals at  $\delta = 107.6, 113.2, 128.4, 128.8, 131.7, 132.8, 135.2, 139.0$  and 145.2 ppm, which are attributed to C≡N group and aromatic carbons, while the carbonyl carbon (C=O) is assigned by signal at  $\delta = 165.5$  ppm.

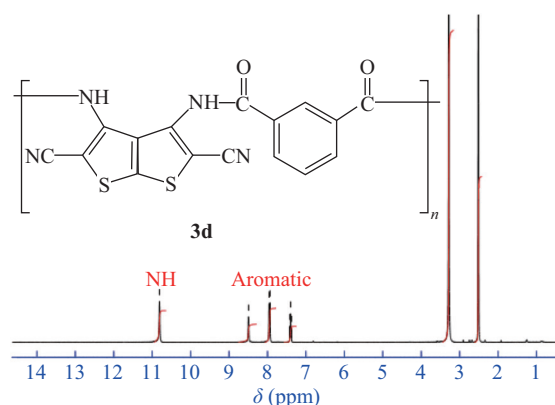


Fig. 2 <sup>1</sup>H-NMR spectrum of polyamide **3d**

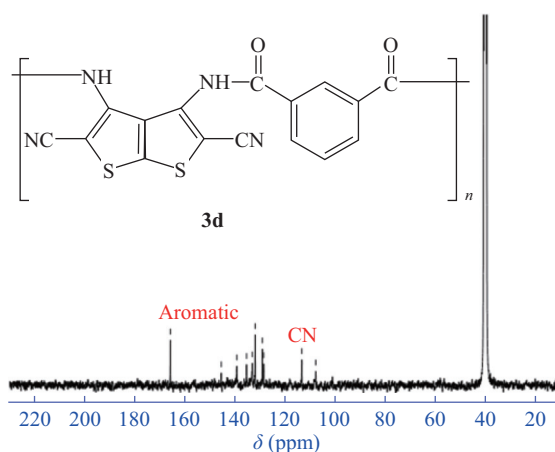


Fig. 3 <sup>13</sup>C-NMR spectrum of polyamide **3d**

### Gel Permeation Chromatography (GPC), Solubility and Inherent Viscosity

The molecular weights and polydispersity index of the synthesized polyamides **3d–3g** were determined by gel permeation chromatography (GPC) (Fig. 4) and are summarized in Table 1. The solubility of the synthesized polyamides **3a–3h** was determined in the polar aprotic solvents such as NMP, DMF, DMSO, CHCl<sub>3</sub>, CHCl<sub>3</sub>/acetone mixture and ethanol (as shown in Table 2). We found that polyamides **3d–3g** are well soluble in the polar aprotic solvents such as DMSO, DMF and NMP. It may be attributed to the rigidity of the aromatic structures and their low crystallinity. On the other hand, the polyamides based on aliphatic methylene linkage exhibited poor solubility. This indicates that they have highly crystalline and symmetrical structure. Moreover, all the obtained polyamides are completely insoluble in chloroform, ethanol or chloroform/acetone mixtures<sup>[22]</sup>. Inherent viscosity was measured at a concentration of 0.5 g·dL<sup>-1</sup> for polyamides **3a–3c** and **3h** in DMF containing 0.5 g·dL<sup>-1</sup> LiCl and for polyamides **3d–3g** in DMF<sup>[4]</sup>.

### Wide Angle X-ray Diffraction (WAXD)

The X-ray diffractograms for selected examples of polyamides **3b**, **3d** and **3g** were measured in the region of  $2\theta = 5^\circ\text{--}60^\circ$  (Fig. 5). The polymer **3d** was amorphous and this was reflected in its excellent solubility. The polymer **3g** was also amorphous containing a halo peak in the region of

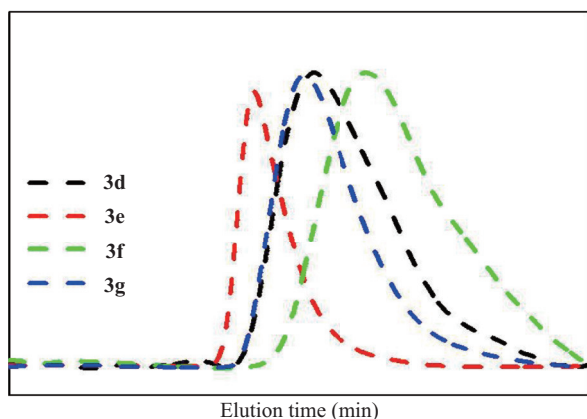


Fig. 4 GPC curves of the polyamides **3d–3g** in DMF as eluent

Table 1 Molecular weights of polyamides **3d–3g** measured through GPC analysis

Sample	$M_n$	$M_w$	PDI
Polyamide <b>3d</b>	$1.09 \times 10^4$	$1.96 \times 10^4$	1.80
Polyamide <b>3e</b>	$1.89 \times 10^4$	$3.13 \times 10^4$	1.70
Polyamide <b>3f</b>	$0.82 \times 10^4$	$1.27 \times 10^4$	1.55
Polyamide <b>3g</b>	$1.18 \times 10^4$	$2.02 \times 10^4$	1.71

$2\theta = 21^\circ\text{--}30^\circ$ . The WAXD profile of polyamide **3b** indicates that it possessed crystalline structure which was attributed to the presence of methylene groups and that leads to increasing flexibility of polymer chain<sup>[38]</sup>.

#### SEM Measurements

The morphologies of the selected examples of the prepared polyamides were examined by scanning electron microscopy (SEM) to show the surface of the polymers and to study the effect of substituents on the surface of the polymer molecules by comparison of images in each case. Figs. 6(a)–6(d) show the SEM images of polyamides **3d**, **3e**, **3f** and **3c**, respectively. It is apparent from Fig. 6(d) that polymer **3c** has a fibrous morphology with a diameter of 0.4–0.6  $\mu\text{m}$  and length up to 4.5–6.5  $\mu\text{m}$ . An appreciable change in morphology has been observed after changing the substituent. As shown in Figs. 6(a)–6(c), the changing from aliphatic to aromatic units for polyamides **3d–3f** resulted in the formation of irregular micro-particles which might consist of bundles of short nanofibers. Polyamides **3d–3f** (See Fig. S12–S14, in ESI) are expected to have high surface area, which enhance their using in diverse applications, for example as corrosion inhibitors. Polyamide **3e** is less porous,

so it has the highest effect on corrosion inhibition and polyamide **3f** has microporous structure, so it might be used in water purification as it is expected to have high adsorption capacity<sup>[39]</sup>.

#### Thermal Gravimetric Analysis (TGA)

The thermal properties of the obtained polyamides **3a–3f** and **3h** were studied *via* thermogravimetric analysis (TGA) under  $\text{N}_2$  atmosphere. All the polyamides showed similar decomposition pattern (three main degradation steps) as shown in Fig. 7. The first region showed mass loss at about 22–200  $^\circ\text{C}$  with insignificant weight loss ranging from 1.5%–5% which may be attributed to loss of moisture and entrapped solvents. The second region for polyamides **3a–3c** showed mass loss at about 110–449  $^\circ\text{C}$  (–17.87%, –17.1%, –27.3% respectively). For polyamides **3d** and **3e** the mass loss was at about 145–417  $^\circ\text{C}$  (–4%, –4.4%, respectively), while for polyamide **3f** and **3h** the mass loss temperature ranged from 149  $^\circ\text{C}$  to 470  $^\circ\text{C}$  (–10%, –20%, respectively). Furthermore the third region showed completely collapsing for the polymer structure. For polyamides **3a** and **3b**, they dissociated in a wide temperature range (420–600  $^\circ\text{C}$ ), while for polyamides **3f** and **3h** at about (470–600  $^\circ\text{C}$ ) and for polyamides **3d** and **3e** at about (500–600  $^\circ\text{C}$ ). The 10% weight loss of the polymer is considered to be the polymer decomposition temperature (PDT)<sup>[40]</sup> (Table 3). According to this temperature we can arrange the polyamides in the order: **3e** > **3d** > **3h** > **3a** > **3f** > **3b** > **3c**. All the previous features confirmed the high thermal stability of the synthesized polymers, but polyamides containing aromatic units are more thermally stable than those prepared from aliphatic diacid chlorides. Polyamide **3c** is less stable than **3b** as the result of increasing the number of methylene groups. These results are in agreement with our previous studies<sup>[22]</sup>.

The polyamides containing cyano group in *ortho* position to –NHCO group undergo thermal degradation *via* intramolecular cyclization to form polybenzoxazole with elimination of HCN<sup>[41]</sup>. In the same manner, the enol form of polyamide **3e** undergoes thermal intramolecular cyclization *via* nucleophilic addition of hydroxyl group on olefinic carbon with elimination of hydrogen cyanide to give polythieno[3,2-*d*]<sup>[1,3]</sup> oxazole (Fig. 8).

TGA thermogram of polyamide **3e** as given in Fig. 9 showed three degradation steps. In the first step, the weight loss can be neglected, attributed to the loss of entrapped solvent and moisture<sup>[22]</sup>. In the second step, the degradation represented loss of HCN (~7 wt%) and formation of

Table 2 Solubility and inherent viscosity of polyamides **3a–3h**

Polymer	NMP	DMF	DMSO	$\text{CHCl}_3$	$\text{CHCl}_3$ + acetone	EtOH	$\eta_{\text{inh}}^*$ (g·dL <sup>–1</sup> )
<b>3a</b>	–	–	–	–	–	–	0.36
<b>3b</b>	–	–	–	–	–	–	0.35
<b>3c</b>	–	–	–	–	–	–	0.38
<b>3d</b>	++	++	++	–	–	–	0.47
<b>3e</b>	++	++	++	–	–	–	0.5
<b>3f</b>	++	++	++	–	–	–	0.3
<b>3g</b>	++	++	++	–	–	–	0.46
<b>3h</b>	–	–	–	–	–	–	0.25

++: Soluble at room temperature (RT); –: Insoluble at room temperature; \*: Inherent viscosity measured at a concentration of 0.5 g·dL<sup>–1</sup> for polyamides **3a–3c** and **3h** in DMF containing 0.5 g/dL LiCl and for polyamides **3d–3g** in DMF.

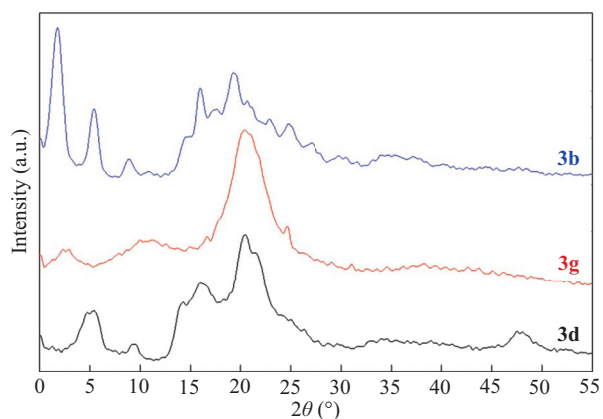


**Fig. 5** WAXD patterns of **3b**, **3d** and **3g**, recorded at room temperature

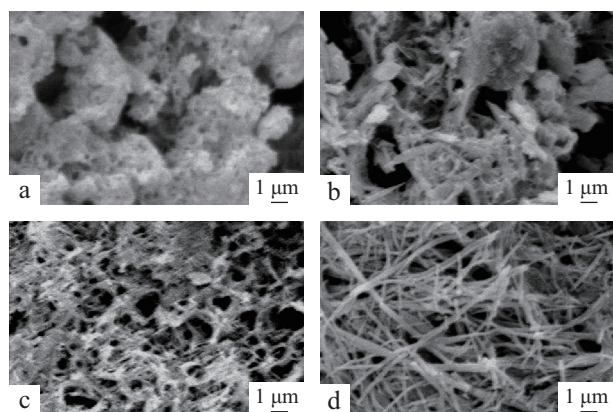


**Fig. 6** SEM images of polyamides **3d** (a), **3e** (b), **3f** (c) and **3c** (d) at magnification  $X = 7500$

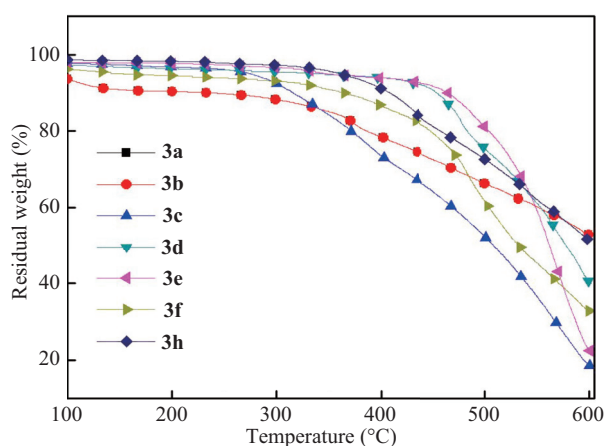


**Fig. 7** TGA curves of polyamides **3a–3f** and **3h** recorded at a heating rate of  $10\text{ °C}/\text{min}$

polythieno[3,2-*d*][1,3]oxazole at  $145\text{--}470\text{ °C}$ . The third step include random degradation of the formed polythieno[3,2-*d*][1,3]oxazole. The DTA curve of **3e** (Fig. 9) showed two  $T_{\text{max}}$  exothermic peaks at  $485\text{ °C}$  due to the loss of HCN and at  $559\text{ °C}$  due to degradation of polythieno[3,2-*d*][1,3]oxazole.

#### Potentiodynamic Polarization Measurements (PDP)

The comparative potentiodynamic polarization curves for carbon steel in  $1\text{ mol}\cdot\text{L}^{-1}$  HCl solution in the absence and

**Table 3** Thermal properties of polyamides **3a–3f** and **3h**

Polymer	Temperature for various percentage decompositions ( $^{\circ}\text{C}$ ) <sup>a</sup>			
	10%	20%	30%	40%
<b>3a</b>	420	457	544	602
<b>3b</b>	385	435	513	589
<b>3c</b>	340	372	420	470
<b>3d</b>	464	488	508	528
<b>3e</b>	470	507	531	550
<b>3f</b>	390	448	481	504
<b>3h</b>	430	457	513	560

<sup>a</sup> The values were determined by TGA at a heating rate of  $10\text{ °C}\cdot\text{min}^{-1}$ .

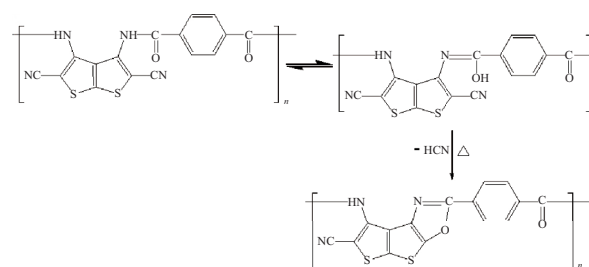


**Fig. 8** The suggested mechanism for thermal degradation of polyamide **3e**

presence of various concentrations of the prepared polymers **3d** and **3e** at  $50\text{ °C}$  are shown in Fig. 10.

It was obvious that both the anodic and cathodic branches displayed lower current density in the presence of the prepared polymers than those listed in the free HCl solutions. This behavior demonstrated that both studied polymers had considerable impacts on both anodic and cathodic corrosion process reactions. The corresponding potentiodynamic polarization parameters such as corrosion current density ( $I_{\text{corr}}$ ), corrosion potential ( $E_{\text{corr}}$ ), anodic and cathodic Tafel slopes ( $\beta_a$ ,  $\beta_c$ ) were estimated from the extrapolation of the cathodic and anodic Tafel lines<sup>[42]</sup>. The inhibition efficiency ( $P_{\text{PDP}}$ ) of the inhibitor was calculated by using  $I_{\text{corr}}$  as follows<sup>[43]</sup>:

$$P_{\text{PDP}}(\%) = \left(1 - \frac{I_{\text{corr}}^i}{I_{\text{corr}}^w}\right) \times 100 = \theta \times 100 \quad (1)$$

where  $I_{\text{corr}}^w$  and  $I_{\text{corr}}^i$  are the corrosion current density values without and with inhibitor, respectively. The calculated polarization parameters along with the percentage of inhibition efficiency ( $P_{\text{PDP}}$ ) are tabulated in Table 4. Examination of the data in Table 4 shows that with the addition of polymers **3d** and **3e** to the aggressive solution, the values of  $I_{\text{corr}}$  decrease significantly, suggesting that both the cathodic reduction of hydrogen ions and anodic dissolution of carbon steel were inhibited. Clearly, more obvious decrease in the  $I_{\text{corr}}$  values was observed at higher concentration of inhibitors. The decrease in the  $I_{\text{corr}}$  observed with the increase of polymer concentration indicates that more inhibitor species are adsorbed on the surface of steel. This means the increase of the surface coverage of metal.

As shown in Table 4, the anodic ( $\beta_a$ ) and cathodic slopes ( $\beta_c$ ) are not changed considerably; the polymer inhibitors simply block the cathodic and anodic reaction sites, and follow the same inhibition mechanism of the electrode reactions<sup>[44]</sup>. The addition of the prepared polymers to the

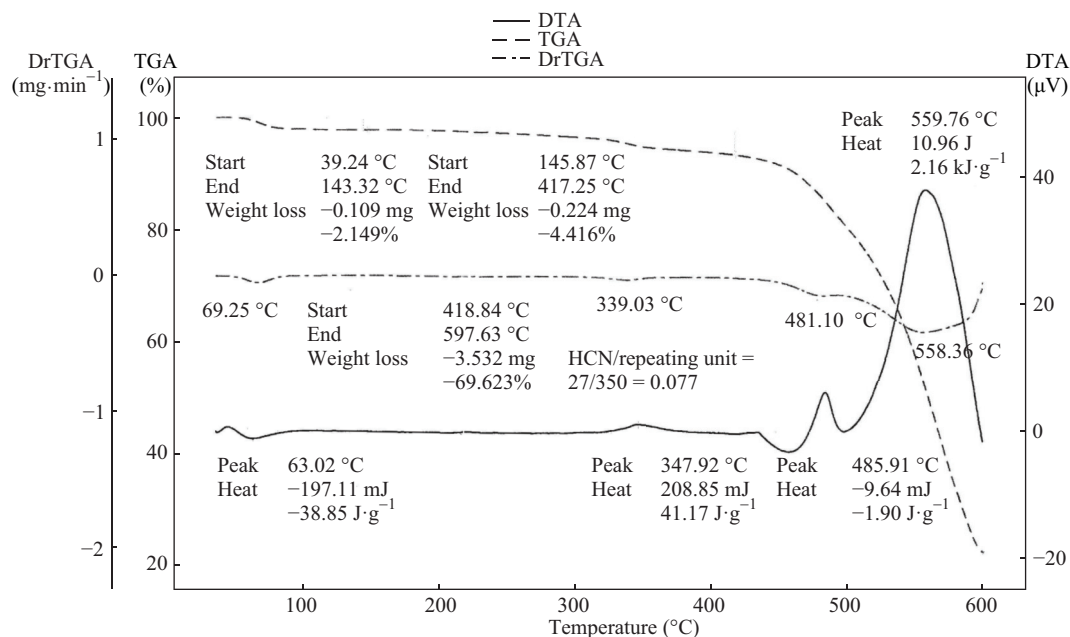


Fig. 9 TGA curves of polyamide **3e** at a heating rate of  $10\text{ }^{\circ}\text{C}\cdot\text{min}^{-1}$

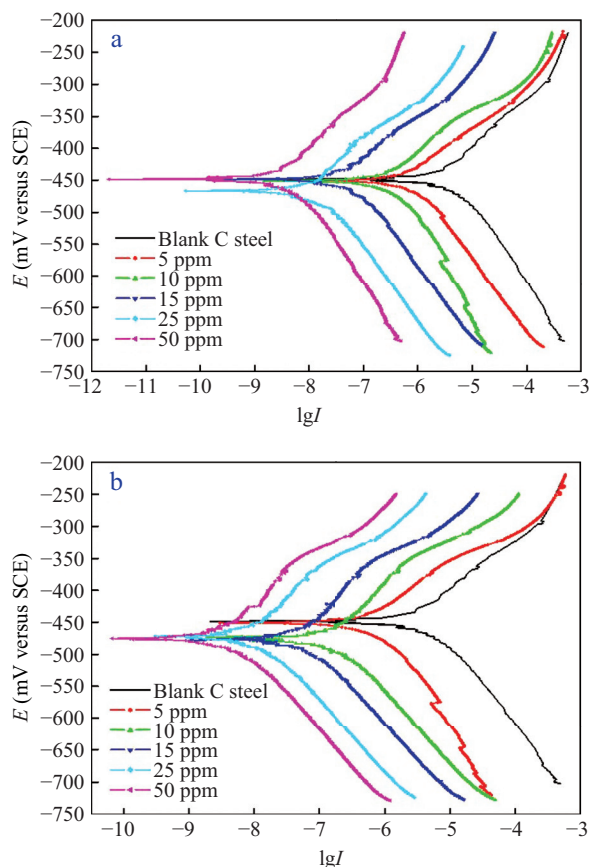


Fig. 10 Potentiodynamic polarization curves of carbon steel in  $1\text{ mol/L HCl}$  solution with or without different concentrations of (a) **3d** and (b) **3e** at  $50\text{ }^{\circ}\text{C}$

acid solutions shifted  $E_{\text{corr}}$  for C-steel between  $1\text{--}19\text{ mV}$  and  $4\text{--}29\text{ mV}$  cathodically for **3d** and **3e** inhibitors, respectively, compared to the blank. In general, if the displacement in  $E_{\text{corr}}$  is more than  $85\text{ mV}$  with respect to  $E_{\text{corr}}$  of the free solution,

the inhibitor can be classified as anodic or cathodic type<sup>[45, 46]</sup>. The obtained results in the investigated study show that **3d** and **3e** polymers act as mixed-type inhibitors with predominantly cathodic inhibition effects. The  $P_{\text{PDP}}$  values for C-steel in  $1\text{ mol}\cdot\text{L}^{-1}\text{ HCl}$  containing  $50\text{ ppm}$  of the studied inhibitors **3d** and **3e** are  $94.51\%$  and  $96.01\%$ , respectively. The higher  $P_{\text{PDP}}$  values in the presence of both investigated polymers indicates that the C-steel is prohibited from direct corrosion attack due to the formation of adsorbed layer from the polymer molecules on the surface of C-steel. This also leads to decrease in the corrosion current density ( $I_{\text{corr}}$ ). It is also evident that the inhibition efficiency of the investigated polymers was found to be nearly the same but slightly increase in the following order: **3e** > **3d**.

The inhibition effect of the monomer **1a** on the corrosion of C-steel in  $1\text{ mol}\cdot\text{L}^{-1}\text{ HCl}$  was performed, in comparison with the inhibition performance of the synthesized polymer inhibitors **3d** and **3e** by potentiodynamic polarization measurements at  $50\text{ }^{\circ}\text{C}$ . It is found that in the presence of  $5$  and  $50\text{ ppm}$  of all studied inhibitors, the  $P_{\text{PDP}}$  values of the monomer compound are  $35.7\%$  and  $69.4\%$ , while the values for **3d** and **3e** are  $67.13\%$ ,  $94.51\%$  and  $68.74\%$ ,  $96.01\%$ , respectively. The higher  $P_{\text{PDP}}$  values of **3d** and **3e** in comparison with the monomer could be due to the large size of the polymers which cover wide area of the steel surface and also due to the presence of more adsorption centers in the polymers than their respective monomers<sup>[47]</sup>.

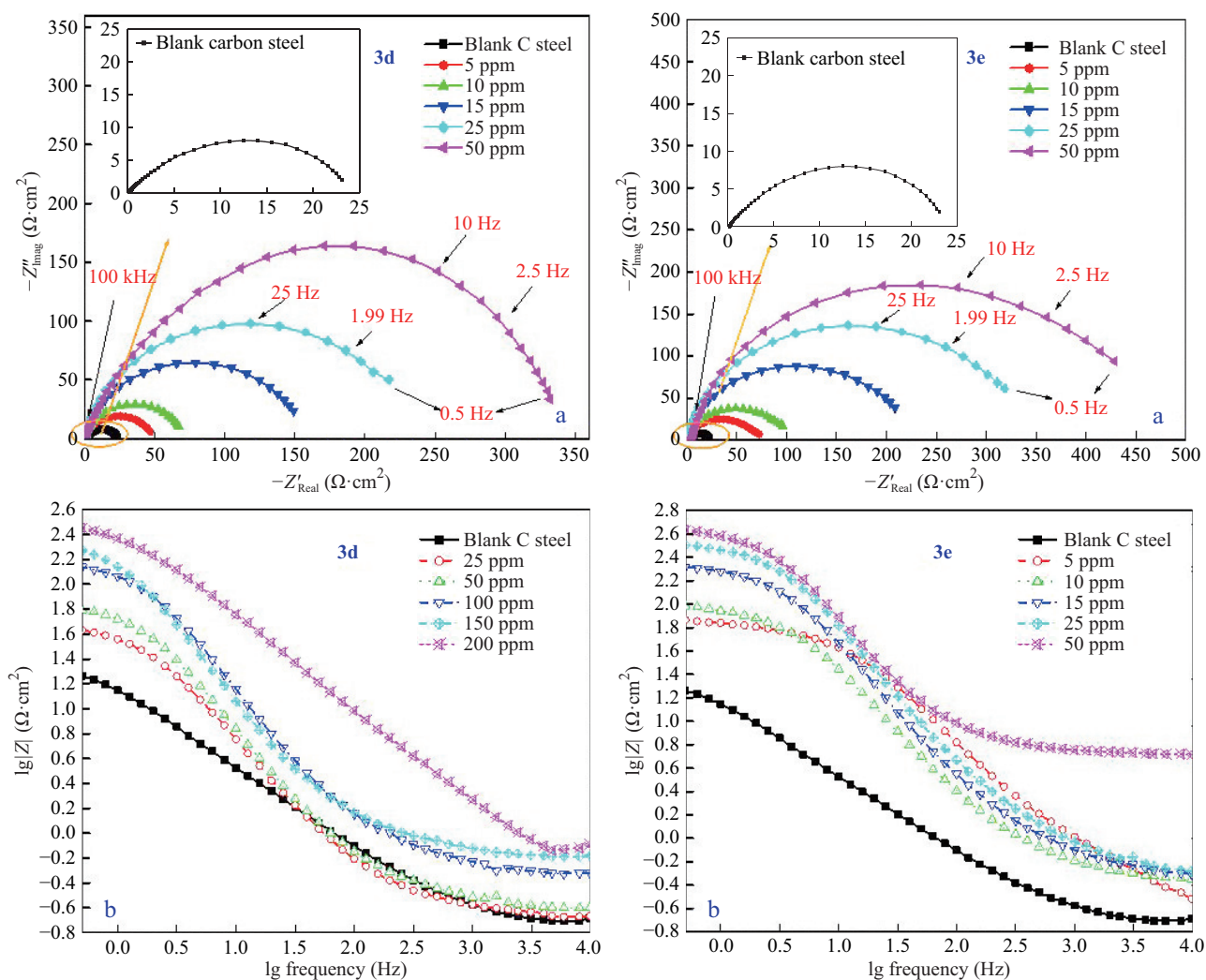
### Electrochemical Impedance Spectroscopy

In order to comprehend the kinetics of the corrosion process and the capacitive conduct of carbon steel electrode in  $1\text{ mol}\cdot\text{L}^{-1}\text{ HCl}$  in the absence and presence of the prepared polymers, EIS measurements were performed. The Nyquist plots for carbon steel in the investigated acid solution containing various concentrations of the studied polymers **3d** and **3e** as corrosion inhibitors are shown in Fig. 11(a). It is



**Table 4** Electrochemical parameters and inhibition efficiency for polyamides **3d** and **3e** obtained from polarization measurements for carbon steel in 1 mol·L<sup>-1</sup> HCl in the absence and presence of various concentrations of polymer inhibitors at 50 °C

Polymer code	$c_{inh}$ (ppm by weight)	$I_{corr}$ ( $\mu\text{A}\cdot\text{cm}^{-2}$ )	$-E_{corr}$ (mV) (SCE)	$\beta_a$ ( $\text{mV}\cdot\text{dec}^{-1}$ )	$-\beta_c$ ( $\text{mV}\cdot\text{dec}^{-1}$ )	$\theta$	$P_{PDP}$ (%)
Blank	0.0	$1231 \pm 78$	448	110	202	–	–
<b>3d</b>	5	$404.6 \pm 35$	452	117	199	0.671	67.13
	10	$329.3 \pm 26$	449	117	212	0.732	73.25
	15	$190.11 \pm 16$	451	114	215	0.845	84.56
	25	$102.9 \pm 10$	467	115	190	0.916	91.64
	50	$67.6 \pm 6$	450	120	207	0.945	94.51
<b>3e</b>	5	$384.8 \pm 40$	452	118	214	0.687	68.74
	10	$316.9 \pm 25$	474	121	208	0.742	74.26
	15	$179.4 \pm 14$	477	117	201	0.854	85.43
	25	$99.3 \pm 8$	472	119	203	0.919	91.93
	50	$49.1 \pm 5$	476	122	207	0.960	96.01

**Fig. 11** Nyquist (a) and (b) Bode modulus plots for carbon steel in 1 mol·L<sup>-1</sup> HCl in the absence and presence of various concentrations of **3d** and **3e** inhibitors at 50 °C

noteworthy that for all the systems the Nyquist plots had the similar shapes, which suggest that introducing inhibitors to the corrosive medium did not cause any significant change in the mechanism of corrosion processes. It is also obvious from Fig. 11(a) that the Nyquist plot diameter increases with increasing polymers concentration which is related to the formation of protective film on the surface of carbon steel leading to obstruction of the corrosion process<sup>[48]</sup>. For a

C-steel/acid system, the replacement of capacitance by the constant phase element (CPE) gives a good approximation<sup>[49]</sup>. CPE can be expressed as<sup>[50]</sup>:

$$Z_{CPE} = \left( \frac{1}{Y_0} \right) [(j\omega)^n]^{-1} \quad (2)$$

where  $j$  is the imaginary number,  $\omega$  is the angular frequency,  $Y_0$  is the CPE constant, and  $n$  is the phase shift, which is

related to the degree of surface inhomogeneity. Based on the value of  $n$ , CPE can represent capacitance ( $n = 1$ ,  $Y_0 = C$ ), resistance ( $n = 0$ ,  $Y_0 = R$ ), inductance ( $n = -1$ ,  $Y_0 = 1/L$ ) or Warburg impedance ( $n = 0.5$ ,  $Y_0 = W$ ). Double layer capacitance ( $C_{dl}$ ) can be estimated as follows<sup>[51]</sup>:

$$C_{dl} = \frac{Y_0(\omega_{max})^{n-1}}{\sin\left(n\left(\frac{\pi}{2}\right)\right)} \quad (3)$$

where  $\omega$  is the angular frequency ( $\omega = 2\pi f_{max}$ ). According to the equivalent circuit in Fig. 12, some impedance parameters such as the charge transfer resistance ( $R_{ct}$ ), the resistance of solution ( $R_s$ ), and the constant phase element (CPE) were estimated, and are listed in Table S1 (in ESI). Similar equivalent circuit has been described in the literature for the acidic corrosion inhibition of steel<sup>[52–54]</sup>. The inhibition efficiency ( $P_{EIS}$ ) of the investigated polymers is calculated by using charge transfer resistance ( $R_{ct}$ ) according to the following equation<sup>[55]</sup>:

$$P_{EIS}(\%) = \left(1 - \frac{R_{ct}^0}{R_{ct}^i}\right) \times 100 \quad (4)$$

where  $R_{ct}^0$  and  $R_{ct}^i$  are the charge transfer resistance in absence and presence of the inhibitors, respectively. It was evident that the values of  $R_{ct}$  in the solutions containing studied inhibitors were permanently greater than their values in the absence of the inhibitors, as  $R_{ct}$  for blank HCl solution was equal to  $24.5 \Omega \cdot \text{cm}^2$  while  $R_{ct} = 353.6$  and  $516.2 \Omega \cdot \text{cm}^2$  in the presence of 50 ppm of **3d** and **3e**, respectively, at 50 °C. Also Bode phase plots in Fig. 11(b) display that the value of impedance in the presence of both polymers is higher than that in uninhibited solution and the impedance value increases on increasing the concentration of investigated polymers. These indicate a reduction in the corrosion rate of steel in presence of both the inhibitors and continuously diminishing on increasing the inhibitor concentrations. The data in Table S1 (in ESI) show that the inhibition efficiency ( $P_{EIS}$ ) values increase with increase in the concentration of the inhibitors. The increase of  $P_{EIS}$  value in the presence of both polymers is related to the formation of protective adsorption film on the surface of carbon steel, which insulates the electrode from the aggressive attack of the acid solution<sup>[56]</sup>. From Table S1 (in ESI), it can be seen that, addition of the prepared polymers provided lower  $C_{dl}$  values, probably as a consequence of replacement of water molecules by inhibitor molecule at the surface of steel.  $C_{dl}$  values decrease with increasing the concentration which may be due to an increase in the thickness of the electrical double layer and/or a decrease in the dielectric constant<sup>[57]</sup>. The  $P_{PDP}$

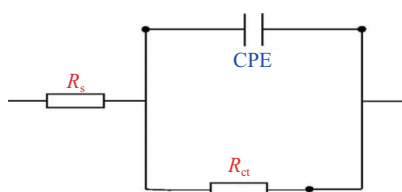


Fig. 12 Electrical equivalent circuit used in fitting the experimental impedance data

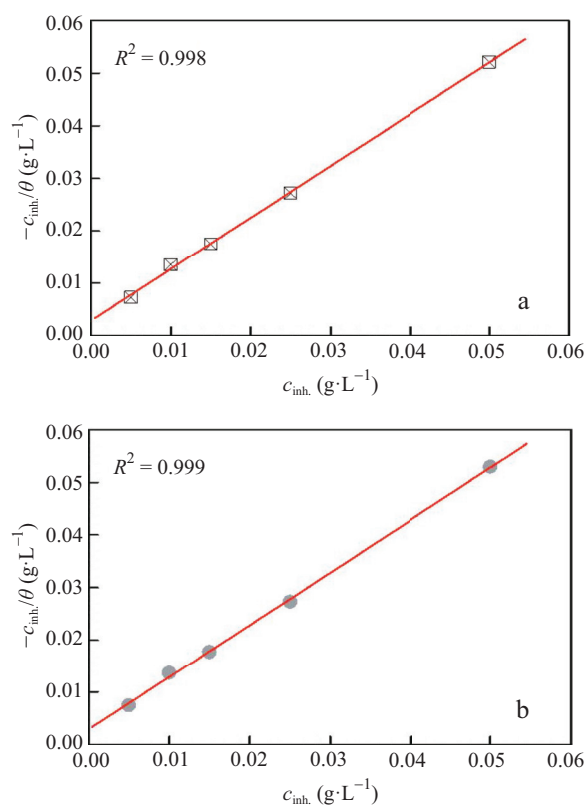


Fig. 13 Langmuir isotherm adsorption model of **3d** (a) and **3e** (b) on the carbon steel surface in  $1.0 \text{ mol} \cdot \text{L}^{-1}$  HCl at 50 °C

values calculated from potentiodynamic polarization measurements were close to the  $P_{EIS}$  values found in EIS measurements. EIS and PDP measurements were repeated at least for 3 times and observed that the results were reproducible.

#### Adsorption Isotherm and Inhibition Mechanism

In order to give more information about the interaction between polymer inhibitor and metal surface, adsorption isotherms were explored. The experimental data were subjected into various adsorption isotherms including Langmuir, Frumkin, Temkin, Bockris-Swinkels, Freundlich, and Flory-Huggins isotherms. By far, Langmuir adsorption isotherm gave the best fit<sup>[41]</sup>:

$$\frac{c_{inh}}{\theta} = c_{inh} + \frac{1}{K_{ads}} \quad (5)$$

where  $c_{inh}$  is molar concentration of inhibitor in the bulk solution,  $K_{ads}$  is the equilibrium constant for the adsorption-desorption process,  $\theta$  is the surface coverage degree.

The  $\theta$  values obtained from polarization measurements for **3d** and **3e** polymer inhibitors were tested graphically by fitting into a suitable adsorption isotherm as indicated in Fig. 13. The best fitted straight line was obtained from the plot of  $c_{inh}/\theta$  versus  $c_{inh}$  with a correlation coefficient ( $R^2$ ) of 0.998 and 0.999 for **3d** and **3e** at 50 °C, respectively, and a slope closed to one. This suggests that the adsorption of these polymers on the steel surface obeyed the Langmuir adsorption isotherm. The strong correlation of the Langmuir adsorption isotherm may confirm the validity of this

approach.

It is well known that  $K_{\text{ads}}$  indicates the strength between adsorbent and adsorbate. Large values of  $K_{\text{ads}}$  reveal more adsorption and hence better inhibition efficiency<sup>[49]</sup>. The values of  $K_{\text{ads}}$  calculated from the reciprocal of intercept of isotherm lines for carbon steel at 50 °C were found to be 348 and 351 L·g<sup>-1</sup> for **3d** and **3e**, respectively. The data displayed high value of  $K_{\text{ads}}$ , indicating a strong adsorption and interaction<sup>[48]</sup>. The values of  $K_{\text{ads}}$  are also related to the standard free energy of adsorption ( $\Delta G_{\text{ads}}^{\circ}$ ) based on the following equation<sup>[58]</sup>:

$$K_{\text{ads}} = \frac{1}{55.5} \exp\left(-\frac{\Delta G_{\text{ads}}^{\circ}}{RT}\right) \quad (6)$$

where  $R$  is the universal gas constant. In this investigation, the values of  $\Delta G_{\text{ads}}^{\circ}$  were found to be -26.50 and -26.52 kJ·mol<sup>-1</sup> for **3d** and **3e**, respectively, indicating that the adsorption of investigated surfactants on steel surface is a combination of both physisorption and chemisorption<sup>[59]</sup>. Meanwhile, negative  $\Delta G_{\text{ads}}^{\circ}$  value for the studied polymers indicates a stronger interaction between the polymer molecules and the surface of steel.

Adsorption of polymers on steel surface depends on many factors including planarity of molecules, active sites on surface of metal, mode of adsorption, free lone pairs present on heteroatoms, concentration of inhibitor *etc*<sup>[60]</sup>. At lower concentration, the polymer molecules can be adsorbed on the steel substrate through electrostatic interaction between the protonated polymer molecules and the charged metal surface (physisorption). In addition to the physical adsorption, the polymer compounds may be adsorbed on anodic site *via* lone pair of electrons of heteroatoms and  $\pi$ -electrons of aromatic ring with vacant d orbitals of Fe (chemisorption) which decreased the anodic dissolution of carbon steel. Moreover, the large size and high molecular weight of the polymer molecules highly affect the inhibition efficiency of the inhibitors. The studied polymers have aromatic rings, heteroatoms, long chain, which get adsorbed on metal surface and form a layer to prevent direct contact of metal with aggressive solution and slow down corrosion rate of carbon steel<sup>[61]</sup>.

## CONCLUSIONS

In this study, we have synthesized novel polyamides containing thieno[2,3-*b*]thiophene moiety *via* a facile method with high yield. The chemical structures of monomer **1a**, model compound **2a** and the synthesized polyamides were confirmed by FTIR, <sup>1</sup>H-NMR, <sup>13</sup>C-NMR and elemental analysis. The solubility, inherent viscosity, crystallinity, surface morphology and thermal stabilities of synthesized polyamides were carefully studied and characterized. In addition, the potentiodynamic polarization and electrochemical measurements revealed that the polyamides containing thieno[2,3-*b*]thiophene moiety can act as mixed-type inhibitors with the inhibition efficiency ( $P$ ) in the range 67.13%–96.01%. We expect that these materials can be used as inhibitors for industrial application.

## Electronic Supplementary Information

Electronic supplementary information (ESI) is available free of charge in the online version of this article at <http://dx.doi.org/10.1007/s10118-018-2101-3>.

## REFERENCES

- 1 Yang, H. H. "Aromatic high-strength fibers", John Wiley & Sons, New York, 1989.
- 2 Liou, G. S.; Yen, H. J. "Polyimides", in: K. Matyjaszewski, M. Moller (eds.), "Polymer science: a comprehensive reference", Elsevier Science, Amsterdam, 2012, P. 497–535.
- 3 Liaw, D. J.; Wang, K. L.; Huang, Y. C.; Lee, K. R.; Lai, J. Y.; Ha, C. S. Advanced polyimide materials: synthesis, physical properties and application. *Prog. Polym. Sci.* 2012, 37, 907–974.
- 4 Hsiao, S. H.; Peng, S. C.; Kung, Y. R.; Leu, C. M.; Lee, T. M. Synthesis and electro-optical properties of aromatic polyamides and polyimides. *Eur. Polym. J.* 2015, 73, 50–60.
- 5 Levchik, S. V.; Weil, E. D. Combustion and fire retardancy of aliphatic nylons. *Polym. Int.* 2000, 49, 1033–1073.
- 6 Wang, Y. F.; Chen, T. M.; Li, Y. J.; Kitamura, M.; Sakurai, I.; Nakaya, T. Studies on syntheses and properties of novel polyamides containing phosphatidyl choline analogous moieties by interfacial polycondensation. *J. Polym. Sci., Part A: Polym. Chem.* 1997, 35, 3065–3074.
- 7 Ferrero, E.; Espeso, J. F.; de La Campa, J. G.; De Abajo, J.; Lozano, A. E. Synthesis and characterization of aromatic polyamides containing alkylphthalimido pendent groups. *J. Polym. Sci. A: Polym. Chem.* 2002, 40, 3711–3724.
- 8 Chen, Y.; Wang, Q. Preparation, properties and characterization of halogen-free nitrogen-phosphorous flame-retarded glass fiber reinforced polyamide 6 composite. *Polym. Degrad. Stab.* 2006, 91, 2003–2013.
- 9 Wang, Q.; Shi, W. Synthesis and thermal decomposition of a novel hyperbranched polyphosphate ester used for flame retardant system. *Polym. Degrad. Stab.* 2006, 91, 1289–1294.
- 10 Liou, G. S.; Hsiao, S. H.; Ishida, M.; Kakimoto, M.; Imai, Y. Synthesis and characterization of novel soluble triphenylamine-containing aromatic polyamides based on *N,N'*-bis(4-aminophenyl)-*N,N'*-diphenyl-1,4-phenylene diamine. *J. Polym. Sci., Part A: Polym. Chem.* 2002, 40, 2810–2818.
- 11 Chern, Y. T.; Wang, W. L. Synthesis and properties of new polyamides based on diamantine. *Macromolecules* 1995, 28, 5554–5560.
- 12 Liou, G. S.; Oishi, Y.; Kakimoto, M. A.; Imai, Y. Preparation and properties of aromatic polyamides from 2,2'-bibenzoic acid and aromatic diamines. *J. Polym. Sci., Part A: Polym. Chem.* 1991, 29, 995–1000.
- 13 Cimecioglu, A. L.; Weiss, R. A. Synthesis and properties of polyamides of 3,3'-dimethyl naphthidine and its model compounds. *J. Polym. Sci., Part A: Polym. Chem.* 1992, 30, 1051–1060.
- 14 Yang, C. P.; Lin, J. H. Preparation and properties of aromatic polyamides and polyimides derived from 3,3-bis[4-(4-amino phenoxy)phenyl]phthalide. *J. Polym. Sci., Part A: Polym. Chem.* 1994, 32, 423–433.
- 15 Jadhav, J. Y.; Preston, J.; Krigbaum, W. R. Aromatic rigid chain copolymers. 1. Synthesis, structure and solubility of phenyl-substituted para-linked aromatic random copolyamides. *J. Polym. Sci. Part A: Polym. Chem.* 1989, 27, 1175–1195.
- 16 Delaviz, Y.; Gungor, A.; MacGrath, J. E.; Gibson, H. W. Soluble phosphine oxide containing aromatic polyamides. *Polymer* 1993, 34, 210–213.
- 17 Takayangi, M.; Katoyse, T. *n*-substituted poly(*p*-phenylene terephthalamide). *J. Polym. Sci. Part A: Polym. Chem.* 1981,

- 19, 1133–1145.
- 18 Itamura, S.; Yamada, M.; Tamura, S.; Matsumoto, T.; Kurosaki, T. Soluble polyimides with polyalicyclic structure. 1. Polyimides from bicyclo [2.2.2]oct-7-ene-2-exo,3-exo,5-exo,6-exo-tetracarboxylic 2,3:5,6-dianhydrides. *Macromolecules* 1993, 26, 3490–3493.
- 19 Bottino, F. A.; Pasquale, G. D.; Pollicino, A.; Scalia, L. Synthesis and characterization of new polyamides containing 6,6' methylenediquinoline units. *Polymer* 1998, 39(20), 4949–4954.
- 20 Morgan, P. "Condensation polymers by interfacial and solution method", John Wiley & Sons, New York, 1965.
- 21 Morgan, P. W.; Kwolek, S. L. Polyamides from phenylenediamines and aliphatic diacids. *Macromolecules* 1975, 8(2), 104–111.
- 22 Aly, K. I.; Hussein, M. A. Synthesis, characterization and corrosion inhibitive properties of new thiazole based polyamides containing diarylidencyclohexanone moiety. *Chinese J. Polym. Sci.* 2015, 33(1), 1–13.
- 23 Liou, G. S.; Maruyama, M.; Kakimoto, M. A.; Imai, Y. Preparation and properties of aromatic polyamides from 2,2'-bis(*p*-aminophenoxy) biphenyl or 2,2'-bis(*p*-aminophenoxy)-1,1'-binaphthyl and aromatic dicarboxylic acids. *J. Polym. Sci., Part A: Polym. Chem.* 1993, 31, 2499–2506.
- 24 Park, S. H.; Lee, J. W.; Suh, D. H.; Ju, S. Y. Synthesis and characteristics of novel polyamides having pendent *N*-phenyl imide groups. *J. Macromol. Sci. A: Pure Appl. Chem.* 2001, 38, 513–525.
- 25 Sarjadi, M. S.; Yi, H.; Iraqi, A.; Lidzey, D. G. Theinothiophene units properties on the carbazole-based polymers for organic solar cell devices. *Malaysian J. Analyt. Sci.* 2015, 19(6), 1205–1217.
- 26 Diez, A. S.; Saidman, S.; Garay, R. O. Synthesis of a theinothiophene conjugated polymer. *Molecules* 2000, 5(3), 555–556.
- 27 Aly, K. I.; Abdel Rahman, M. A.; Hussein, M. A. New polymer syntheses Part 53. Novel polyamides of diarylidencycloalkane containing azo groups in the polymer backbone: synthesis and characterization. *Int. J. Polym. Mater.* 2010, 59, 553–569.
- 28 Chao, D.; He, L.; Berda, E. B.; Wang, S.; Jia, X.; Wang, C. Multifunction hyperbranched polyamide: synthesis and properties. *Polymer* 2013, 54, 3223–3229.
- 29 Faghihi, K. New polyamides based on bis (*p*-amidobenzoic acid)-*p*-phenylene diacrylic acid and hydantoin derivatives: synthesis and characterization. *Turk. J. Chem.* 2008, 32, 75–86.
- 30 Bair, T. I.; Morgan, P. W.; Killian, F. L. Poly(1,4-phenyleneterephthalamides). polymerization and novel liquid-crystalline solutions. *Macromolecules* 1977, 10(6), 1396–1400.
- 31 Vogel, A. I. "Vogel's textbook of practical organic Chemistry". London, Longman Green 1, 1967, p. 464.
- 32 Aly, K. I. New polymer syntheses XXVIII. Synthesis and thermal behavior of new organometallic polyketones and copolyketones based on diferrocenyldencyclohexanone. *J. Appl. Polym. Sci.* 2004, 94, 1440–1448.
- 33 Aly, K. I.; Kandeel, M. M. New Polymer Syntheses IV. Synthesis and characterization of new polyamides containing bis-benzthiazolyl sulphone units in the main chain. High perform. *Polym.* 1996, 8, 307–314.
- 34 El-Shafei, A. K.; Abdel-Ghany, H. A.; Sultan, A. A.; El-Saghier, A. M. M. Synthesis of thieno (2,3-*b*) thiophene and related structures. *Phosphorus, Sulfur, Silicon Relat. Elem.* 1992, 73, 15–25.
- 35 Comel, A.; Kirsch, G. Efficient one pot preparation of variously substituted thieno[2,3-*b*]thiophene. *J. Heterocycl. Chem.* 2001, 38, 1167–1171.
- 36 Yamazaki, N.; Matsumoto, M.; Higashi, F. Studies on reactions of the *N*-phosphonium salts of pyridines. XIV. Wholly aromatic polyamides by the direct polycondensation reaction by using phosphites in the presence of metal salts. *J. Polym. Sci., Part A: Polym. Chem.* 1975, 13, 1373–1380.
- 37 Holmer, D. A.; Pickett, O. A.; Saunders, J. H. Melt polycondensation of 4,4'-diaminodiphenylmethane with aliphatic dibasic acids. *J. Polym. Sci., Part A: Polym. Chem.* 1972, 10, 1547–1552.
- 38 Li, C. H.; Chang, T. C. Studies on thermotropic liquid crystalline polymers Part II. Synthesis and properties of poly(azomethine-ether). *Eur. Polym. J.* 1991, 27(1), 35–39.
- 39 Yang, R. X.; Wang, T. T.; Deng, W. Q. Extraordinary capability for water treatment achieved by a perfluorous conjugated microporous polymer. *Sci. Rep.* 2015.
- 40 Aly, K. I. New polymer syntheses VIII. Synthesis, characterization and morphology of new unsaturated copolyesters based on dibenzylidencycloalkanones. *Polym. Int.* 1998, 47, 483–490.
- 41 Kim, S.; Pearce, E. M.; Kwei, T. K. Synthesis and degradation of cyano-containing aramids. *Polym. Adv. Technol.* 1990, 1, 49–73.
- 42 El-Sayed, A. R.; Shaker, A. M.; Abd El-Lateef, H. M. Corrosion inhibition of tin, indium and tin-indium alloys by adenine or adenosine in hydrochloric acid solution. *Corros. Sci.* 2010, 52, 72–81.
- 43 Abd El-Lateef, H. M. Experimental and computational investigation on the corrosion inhibition characteristics of mild steel by some novel synthesized imines in hydrochloric acid Solutions. *Corros. Sci.* 2015, 92, 104–117.
- 44 Al-Sabagh, A. M.; Nasser, N. M.; El-Azabawy, O. E.; El-Tabey, A. E. Corrosion inhibition behavior of new synthesized nonionic surfactants based on amino acid on carbon steel in acid media. *J. Mol. Liq.* 2016, 219, 1078–1088.
- 45 Kosari, A.; Moayed, M. H.; Davoodi, A.; Parvizi, R.; Momeni, M.; Eshghi, H.; Moradi, H. Electrochemical and quantum chemical assessment of two organic compounds from pyridine derivatives as corrosion inhibitors for mild steel in HCl solution under stagnant condition and hydrodynamic flow. *Corros. Sci.* 2014, 78, 138–150.
- 46 Yadav, D. K.; Quraishi, M. A. Electrochemical investigation of substituted pyranopyrazoles adsorption on mild steel in acid solution. *Ind. Eng. Chem. Res.* 2012, 51, 8194–8210.
- 47 Morad, M. S. Corrosion inhibition of mild steel in sulfamic acid solution by S-containing amino acids. *J. Appl. Electrochem.* 2008, 38, 1509–1518.
- 48 Abd El-Lateef, H. M.; Abu-Dief, A. M.; El-Gendy, B. E. M. Investigation of adsorption and inhibition effects of some novel compounds towards mild steel in H<sub>2</sub>SO<sub>4</sub> solution: Electrochemical and theoretical quantum studies. *J. Electroanal. Chem.* 2015, 758, 135–147.
- 49 Abd El-Lateef, H. M.; Abu-Dief, A. M.; Abdel-Rahman, L. H.; Sañudo, E. C.; Aliaga-Alcalde, N. Electrochemical and theoretical quantum approaches on the inhibition of C1018 carbon steel corrosion in acidic medium containing chloride using some newly synthesized phenolic Schiff bases compounds. *J. Electroanal. Chem.* 2015, 743, 120–133.
- 50 Mazumder, M. A. J.; Nazal, M. K.; Faiz, M.; Ali, Shi. A.. Midazolines containing single-, twin- and triple- tailed hydrophobes and hydrophilic pendants (CH<sub>2</sub>CH<sub>2</sub>NH)<sub>n</sub> as inhibitors of mild steel corrosion in CO<sub>2</sub> -0.5 M NaCl. *RSC Adv.* 2016, 6, 12348–12362.
- 51 Ansari, K. R.; Quraishi, M. A. Isatin derivatives as a non-toxic corrosion inhibitor for mild steel in 20% H<sub>2</sub>SO<sub>4</sub>. *Corros. Sci.* 2015, 95, 62–70.
- 52 Atta, A. M.; El-Azabawy, O. E.; Ismail, H. S.; Hegazy, M. A. Novel dispersed magnetite core-shell nanogel polymers as corrosion inhibitors for carbon steel in acidic medium. *Corros. Sci.* 2011, 53, 1680–1689.
- 53 Prabhu, R. A.; Venkatesha, T. V.; Shanbhag, A. V.; Kulkarni,

- G. M.; Kalkhambkar, R. G. Inhibition effects of some Schiff's bases on the corrosion of mild steel in hydrochloric acid solution. *Corros. Sci.* 2008, 50, 3356–3362.
- 54 Elayyachy, M.; El Idrissi, A.; Hammouti, B. New thio-compounds as corrosion inhibitor for steel in 1 M HCl. *Corros. Sci.* 2006, 48, 2470–2479.
- 55 Singh, A.; Lin, Y.; Obot, I. B.; Ebenso, E. E.; Ansari, K. R.; Quraishi, M. A. Corrosion mitigation of J55 steel in 3.5% NaCl solution by a macrocyclic inhibitor. *Appl. Surf. Sci.* 2015, 356, 341–347.
- 56 Roy, P.; Karfa, P.; Adhikar, U.; Sukul, D. Corrosion inhibition of mild steel in acidic medium by polyacrylamide grafted Guar gum with various grafting percentage: Effect of intramolecular synergism. *Corros. Sci.* 2014, 88, 246–253.
- 57 Gopi, D.; Karthikeyana, P.; Kavithac, L.; Surendiran, M. Development of poly (3,4-ethylenedioxythiophene-co-indole-5-carboxylic acid) co-polymer coatings on passivated low-nickel stainless steel for enhanced corrosion resistance in the sulphuric acid medium. *Appl. Surf. Sci.* 2015, 357, 122–130.
- 58 Abd El-Lateef, H. M.; Tantawy, A. H. Synthesis and evaluation of novel series of Schiff base cationic surfactants as corrosion inhibitors for carbon steel in acidic/chloride media. *RSC Adv.* 2016, 6, 8681–8700.
- 59 Abd El-Lateef, H. M.; Tantawy, A. H.; Abdelhamid, A. A. Novel quaternary ammonium- based cationic surfactants: Synthesis , surface activity and evaluation as corrosion inhibitors for C1018 carbon steel in acidic chloride solution. *J. Surfact. Deterg.* 2017, 20, 735–753.
- 60 Abd El-Lateef, H. M.; Soliman, K. A.; Tantawy, A. H. Novel synthesized Schiff base-based cationic Gemini surfactants: Electrochemical investigation, theoretical modeling and applicability as biodegradable inhibitors for mild steel against acidic corrosion. *J. Mol. Liq.* 2017, 232, 478–498.
- 61 Abd El-Lateef, H. M.; Elremaily, M. A. A. Divinyl sulfone cross-linked  $\beta$ -cyclodextrin polymer as new and effective corrosion inhibitor for Zn anode in 3.5 M KOH. *Trans. Indian Inst. Met.* 2016, 69(9), 1783–1792.